Upgrading Voltage Control Method Based on Photovoltaic Penetration Rate

Satoru Akagi, *Student Member, IEEE*, Ryo Takahashi, Akihisa Kaneko, Masakazu Ito, Jun Yoshinaga, Yasuhiro Hayashi, *Member, IEEE*, Hiroshi Asano, *Member, IEEE*, and Hiromi Konda

***Abstract*—In this paper, we propose a comprehensive scheme to determine a suitable method and timing for upgrading the voltage control method. Voltage control methods are expected to be upgraded in accordance with the photovoltaic (PV) penetration in distribution systems. The suitable method and timing detailed in this paper are based on the limit of the PV penetration rate, which is constrained by the regulated voltage deviation. The upgrade process involves moving the on-load tap changer (OLTC) control method from the conventional scalar line drop compensator (LDC) method to the vector LDC method or centralized control method. Then, a static var compensator (SVC) or step voltage regulator (SVR) is installed. The locations of the SVR and SVC are determined to maximize the PV penetration rate. The suitable method and timing are demonstrated using a general distribution system. In addition to the numerical simulations, experiments are performed using an active network system with energy resources. The experimental results are consistent with the numerical simulation results, thus validating the proposed scheme. The maximum PV penetration rate obtained using the OLTC control method is 55%. Whereas, the installation of the SVR and SVC increased the rate to 95% and 100%, respectively.**

***Index Terms*—Line drop compensator (LDC), on-load tap changer (OLTC), photovoltaic (PV) system, static var compensator (SVC), step voltage regulator (SVR).**

I. Introduction

THE USE of photovoltaic (PV) systems is continually increasing worldwide. In 2014, the cumulative solar electricity capacities installed by the United States, Germany, and Japan were 20 GW, 38.2 GW, and 23.2 GW, respectively [1]. The PV capacity increased by approximately 40 GW in 2014. Close to half of the new PV capacities were installed in Asia, including China (10 GW) and Japan (9 GW) [2]. Furthermore, in Japan, the number of PV systems has rapidly increased due to the feed-in tariff enforced in 2012.

The capacity of installed PV systems reached approximately 34.1 GW (8.8 GW for households and 25.3 GW for non-households) by the end of June 2016 [3]. PV systems for households have been connected to the distribution systems. The Japanese government has set a goal of installing 28 GW PV systems by 2020 and 64 GW by 2030 [4]. It is assumed that the penetration of PV systems into distribution systems will continue to increase.

Studies on the hosting capacity of PV systems and novel voltage control methods have been conducted previously. Hosting capacity calculations are necessary in planning voltage control systems. In [5]–[11], hosting capacities under various situations were reported. In [5] specifically, hosting capacities under various PV system deployments with existing voltage control methods and infrastructure configurations were calculated in terms of voltage regulation and protection of feeders. Wang *et al.* [7] proposed an evaluation method for maximum hosting capacity (MHC) considering the optimal operation of on-load tap changers (OLTCs) and static var compensators (SVCs). The authors discussed a method of determining the critical technical restrictions on MHC. Moreover, Jayasekara *et al.* [8] employed a battery energy storage system to increase the hosting capacity of distributed generation and proposed a number of voltage control methods. In their approaches, reverse power flow from PV systems raises the distribution voltage at high PV penetration levels.

Currently, distribution voltage is primarily controlled using tap changer transformers, such as the OLTC and step voltage regulators (SVRs). However, the conventional voltage control method for tap changers assumes only a load current without reverse power flow. Thus, the tap changer may be unable to maintain the distribution voltage within an admissible range when the PV penetration is high [12]. Several methods have been proposed to resolve the voltage rise problem [12]–[23]. Yorino *et al.* [13] proposed a voltage control method for tap controllers in distribution systems with high PV penetration based on a multi-agent system. The results of numerical simulations showed that an increase in PV systems penetration causes frequent tap changing operations and distribution voltage deviations with a conventional voltage control method. On the other hand, their proposed method realized optimal tap control by adding the function to the conventional tap controllers.

Manuscript received November 23, 2015; revised April 3, 2016 and August 20, 2016; accepted November 3, 2016. Date of publication December 28, 2016; date of current version August 21, 2018. This work was supported by the Ministry of Economy, Trade and Industry. Paper no. TSG-01482-2015.

S. Akagi is with the Graduate School of Advanced Science and Engineering, Waseda University, Tokyo 169-8555, Japan (e-mail: 1k1gi-s1toru@akane.waseda.jp).

R. Takahashi is with the Graduate School of Electrical Engineering and Bioscience, Waseda University, Tokyo 169-8555, Japan (e-mail: ryo1990915@akane.waseda.jp).

A. Kaneko, Y. Hayashi, and H. Asano are with the Department of Electrical Engineering and Bioscience, Waseda University, Tokyo 169-8555, Japan (e-mail: a-kaneko.0811@fuji.waseda.jp; hayashi@waseda.jp).

M. Ito and J. Yoshinaga are with the Advanced Collaborative Research Organization for Smart Society, Waseda University, Tokyo 169-8555, Japan (e-mail: ito.m@aoni.waseda.jp; j.yoshinaga@kurenai.waseda.jp).

H. Konda is with TEPCO Power Grid, Inc., Tokyo 100-8560, Japan (e-mail: konda.hiromi@tepco.co.jp).

Color versions of one or more of the figures in this paper are available online at http://ieeexplore.ieee.org.

Digital Object Identifier 10.1109/TSG.2016.2645706

Another problem of using PV systems is that their output fluctuates significantly with respect to weather conditions, which may cause voltage deviations in distribution systems.

A tap changer cannot follow rapid voltage fluctuations on account of a working delay function that prevents life span deterioration [24]. To manage the fluctuating voltage, previous researchers have proposed control methods that use equipment that output reactive power (e.g., SVCs and shunt capacitors) [25]–[34]. In [25] for example, a distribution static compensator (DSTATCOM) was employed for voltage regulation to increase the PV hosting capacity of a distribution system. Using this method, the optimal PV hosting capacity was determined by maximizing the net present value.

As described in the foregoing, many studies have been conducted on hosting capacity and voltage control methods. In addition, selecting a suitable method and timing is important for upgrading the voltage control method to increase PV penetration in distribution systems without excessive capital investments or voltage deviations due to transition delays. To date, however, no study has been reported on upgrading the voltage control method. Generally, upgrading the voltage control method is required along with increasing PV penetration. Thus, we propose an approach to determine a suitable method and timing for upgrading the voltage control methods based on the limit of the PV penetration rate. This limit was determined by numerical simulations and experiments using a distribution system model of a residential area. A numerical simulation was used to evaluate various simulation conditions, and experiments validated the simulation results. The proposed approach may thus contribute toward the planning of voltage control in distribution systems and the increasing of distributed PV system penetration levels.

The remainder of this paper is organized as follows. Section II explains conventional and upgraded voltage control methods. Section III describes the upgrade process of voltage control methods and the selection of control parameters of the OLTC, SVR, and SVC. Sections IV and V describe the simulation conditions and results of the numerical simulation and experiment, respectively. Section VI presents the study conclusion.

II. Voltage Control Methods

This section explains the conventional voltage control method of OLTC. In addition, two types of upgraded voltage control methods are described: upgrading the OLTC control method, and installing voltage control equipment, such as the SVR and SVC. As mentioned in the Introduction, many voltage control methods using specific equipment have already been proposed. However, the OLTC, SVR, and SVC were selected as the voltage control equipment for the present study based on the results of a questionnaire provided to nearly all the Japanese power companies.

A. Scalar LDC Method (Conventional Method of OLTC)

The scalar LDC method changes the tap position to maintain the calculated voltage of a reference point (reference voltage)

$$V_{\mathrm{ref}}(t) = \left|\dot{V}_{\mathrm{sec}}(t)\right| - \sqrt{3}\left|\dot{I}(t)\right|(R_{\mathrm{ref}}\cos\theta + X_{\mathrm{ref}}\sin\theta) \quad (1)$$

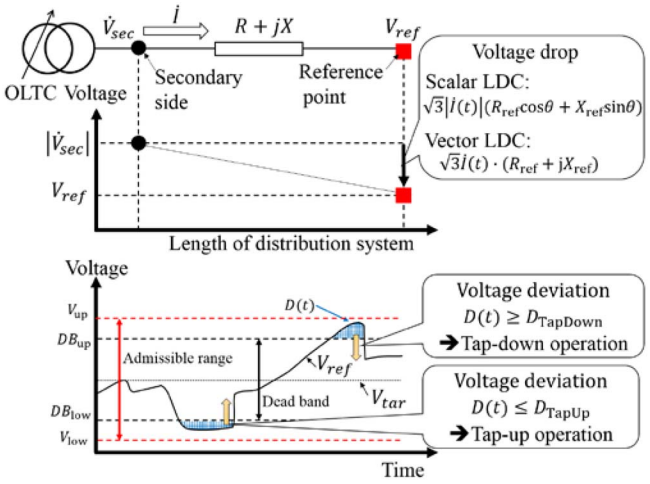

Fig. 1. Scalar and vector LDC methods.

within a dead band. The reference voltage, V_{ref}, is calculated as shown in (1) using the absolute value of the secondary side voltage of the OLTC $|\dot{V}_{\mathrm{sec}}|$, the absolute value of the current passing through the OLTC $|\dot{I}|$ and the simulated line resistance, R_{ref}, and reactance, X_{ref}, with the set lag power factors, $\cos\theta = 0.98$ and $\sin\theta = 0.20$, respectively.

$$D(t) = \begin{cases} D\left(t - t_{\mathrm{step}}\right) + V_{\mathrm{ref}}(t) - DB_{\mathrm{up}}, & \text{if } \left(V_{\mathrm{ref}}(\mathrm{t}) > DB_{\mathrm{up}}\right) \\ D\left(t - t_{\mathrm{step}}\right) + V_{\mathrm{ref}}(t) - DB_{\mathrm{low}}, & \text{if } \left(V_{\mathrm{ref}}(\mathrm{t}) < DB_{\mathrm{low}}\right). \\ 0, & \text{otherwise} \end{cases} \quad (2)$$

$$tap_{\mathrm{change}}\left(t + t_{\mathrm{step}}\right) = \begin{cases} -1, & \text{if } \left(D(\mathrm{t}) \geq D_{\mathrm{TapDown}}\right) \\ +1, & \text{if } \left(D(\mathrm{t}) \leq D_{\mathrm{TapUp}}\right). \\ 0, & \text{otherwise} \end{cases} \quad (3)$$

As shown in (2), the voltage deviation amount, D, is integrated when the reference voltage deviates from the dead band and becomes zero when the reference voltage is within the dead band whose upper and lower limits are DB_{up} and DB_{low}, respectively. The tap is controlled depending on the voltage deviation given by (3), where D_{TapDown} and D_{TapUp} are the voltage deviations for tap-down and tap-up operations, respectively, while tap_{change} is the change in the OLTC tap position. In addition, -1 denotes the tap-down operation, +1, the tap-up operation, and 0, non-operation. In the numerical simulation and experiment, the time step, t_{step}, was set to 60 s.

B. Vector LDC Method (Upgraded Method 1 of OLTC)

$$V_{\mathrm{ref}}(t) = \left|\dot{V}_{\mathrm{sec}}(t) - \sqrt{3}\dot{I}(t) \cdot (R_{\mathrm{ref}} + \mathrm{j}X_{\mathrm{ref}})\right|. \quad (4)$$

When the power factor changes dynamically, the scalar LDC method cannot properly calculate the reference point voltage because of the fixed power factor. In contrast, the vector LDC method provides a more accurate calculation since the vector calculation considers dynamic changes in the power factor.

The vector calculation is represented by (4), which uses the phase of the secondary side voltage, $\dot{V}_{\mathrm{sec}}$, and passing current $\dot{I}$, while j is an imaginary unit. The voltage deviation and tap operation are obtained using (2) and (3). The top of Fig. 1 shows the calculated reference voltage. The scalar LDC

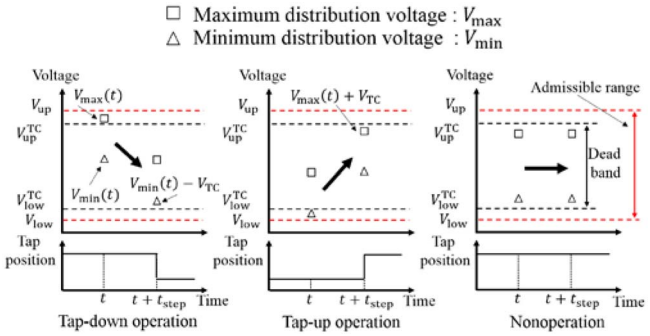

Fig. 2. Centralized control method.

and vector LDC methods used to calculate the reference voltage are represented by (1) and (4), respectively. As shown in the bottom figure, the tap position of the OLTC changes when the voltage deviation D exceeds D_{TapDown} or falls below D_{TapUp}.

C. Centralized Control Method (Upgraded Method 2 of OLTC and SVR)

The centralized control method manages the distribution voltage within an admissible range using the voltage measured at the switches with sensors.

$$tap_{\mathrm{change}}(t+t_{\mathrm{step}}) = \begin{cases} -1, & \text{if } \left(V_{\max}(t) > V_{\mathrm{up}}^{\mathrm{TC}},\ V_{\min}(t) - V_{\mathrm{TC}} \geq V_{\mathrm{low}}^{\mathrm{TC}}\right) \\ +1, & \text{if } \left(V_{\min}(t) < V_{\mathrm{low}}^{\mathrm{TC}},\ V_{\max}(t) + V_{\mathrm{TC}} \leq V_{\mathrm{up}}^{\mathrm{TC}}\right). \\ 0, & \text{otherwise} \end{cases} \tag{5}$$

The tap change of the OLTC and SVR is described in (5). This method uses the maximum and minimum values of the measured voltages as the representative voltages. $V_{\max}$ and $V_{\min}$ are the maximum and minimum distribution voltages, respectively, measured at the switches with sensors, while $V_{\mathrm{up}}^{\mathrm{TC}}$ and $V_{\mathrm{low}}^{\mathrm{TC}}$ are the respective upper and lower limits of the dead band. V_{TC} is the voltage change per tap of the OLTC or SVR.

Fig. 2 shows the tap operation using the maximum and minimum values of the measured voltage. The admissible voltage range is given by V_{up} and V_{low}. The tap position changes when the representative voltage deviates from the dead band before the tap operation and when the voltages after the tap operation are within the dead band (left and middle of Fig. 2). The tap position does not change when voltages after the tap operation are outside the dead band or the distribution voltages are within the dead band (right of Fig. 2).

D. Control Method of SVC

The SVC outputs reactive power to maintain the monitored voltage at the interconnection point to a distribution system within the dead band. The difference between the upper

$$\Delta V_{\mathrm{SVC}}(t) = \begin{cases} V_{\mathrm{SVC}}(t) - V_{\mathrm{up}}^{\mathrm{SVC}}, & \text{if } \left(V_{\mathrm{SVC}}(t) > V_{\mathrm{up}}^{\mathrm{SVC}}\right) \\ V_{\mathrm{SVC}}(t) - V_{\mathrm{low}}^{\mathrm{SVC}}, & \text{if } \left(V_{\mathrm{SVC}}(t) < V_{\mathrm{low}}^{\mathrm{SVC}}\right). \\ 0, & \text{otherwise} \end{cases} \tag{6}$$

$$Q_{\mathrm{SVC}}(t) = \begin{cases} K_{\mathrm{p}}\Delta V_{\mathrm{SVC}}(t) + K_{\mathrm{i}}\int \Delta V_{\mathrm{SVC}}(t)\mathrm{dt}, & \text{if } (\Delta V_{\mathrm{SVC}}(t) \neq 0) \\ Q_0 - K_{\mathrm{a}}\int Q_{\mathrm{i}}(t)\mathrm{dt}, & \text{if } (\Delta V_{\mathrm{SVC}}(t) = 0) \end{cases} \tag{7}$$

(or lower) limit of the dead band and the voltage of the SVC interconnection point, ΔV_{SVC}, is calculated using (6). The SVC outputs the reactive power based on proportional–integral (PI) control (see (7)). When the voltage deviates from the dead band ($\Delta V_{\mathrm{SVC}} \neq 0$), the reactive power output is calculated using the first condition of (7). Conversely, when the monitored voltage is within the dead band ($\Delta V_{\mathrm{SVC}} = 0$), the reactive power output is reduced based on the second condition of (7). In (6) and (7), $V_{\mathrm{up}}^{\mathrm{SVC}}$ is the upper limit of the dead band, $V_{\mathrm{low}}^{\mathrm{SVC}}$ is the lower limit of the dead band, and Q_{SVC} is the reactive power output of the SVC. Furthermore, K_{p} is the proportional gain, K_{i} is the integral gain, K_{a} is the attenuation gain, Q_{i} is the reactive power output of the integrator control unit, and Q_0 is the value of Q_{i} when the voltage of the SVC interconnection point enters the dead band.

III. Upgrade of the Voltage Control Method and Selection of Control Parameters

This section describes the upgrade policy for the voltage control method and the selection of control parameters for the scalar and vector LDC methods and PI control. The control parameters of each voltage control method are determined using the distribution voltage at all nodes to maximize the PV penetration level.

A. Control Parameters Selection for OLTC

To obtain the control performance of the conventional voltage control method, the limit of the PV penetration rate is calculated using the scalar LDC method. The target voltage of the reference point, as well as the simulated line resistance, R_{ref}, and reactance, X_{ref}, comprise the control parameters for the LDC method. The control parameters for the scalar LDC method are determined using the load current with no PV systems.

As the first step of upgrading the voltage control method, the OLTC control method is changed from the scalar LDC to the vector LDC method. This is because the OLTC control method affects the entire distribution system, and upgrading to the vector LDC method does not require introducing new equipment. The control parameters of the vector LDC method are determined as follows. First, the control parameters are determined in a similar manner as the scalar LDC method. Second, when the voltage deviates in the scalar LDC method as the PV penetration rate increases, the conventional control parameters are revised to avoid the voltage deviation. The control parameters of the LDC method are common for each validation day: three days with three types of PV profiles, as shown in Section V, and one day with no PV systems.

$$V_{\mathrm{devi}}(V_{\mathrm{tar}}, R_{\mathrm{ref}}, X_{\mathrm{ref}}) = \sum_{d=1}^{N_{\mathrm{date}}} \sum_{n=1}^{N_{\mathrm{node}}} \sum_{t=1}^{T} \Delta V_{d,n}(t) \cdot t_{\mathrm{step}}. \tag{8}$$

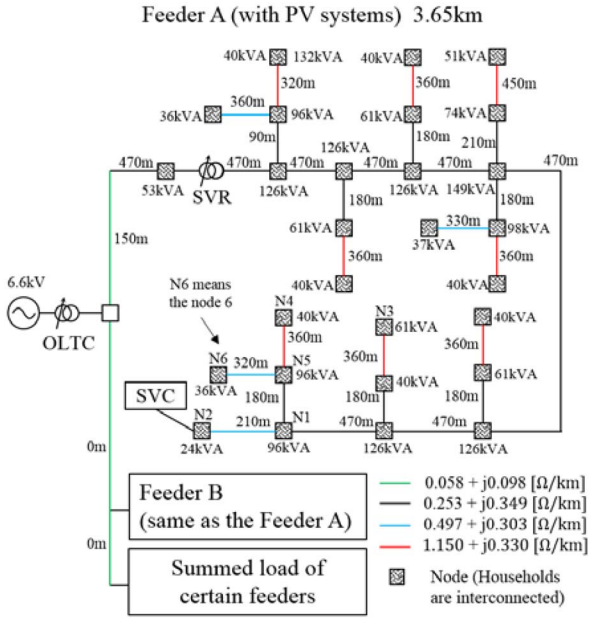

Fig. 3. Distribution system model used for the numerical simulation.

$$\Delta V_{d,n}(t) = \begin{cases} V_{d,n}(t) - V_{\mathrm{up}}, & \text{if } \left(V_{d,n}(t) > V_{\mathrm{up}}\right) \\ \left|V_{d,n}(t) - V_{\mathrm{low}}\right|, & \text{if } \left(V_{d,n}(t) < V_{\mathrm{low}}\right). \\ 0, & \text{otherwise} \end{cases} \tag{9}$$

The control parameters of the scalar and vector LDC methods are determined in such a way as to minimize the sum of the voltage deviations, V_{devi}, as calculated using (8). In (8), N_{date} is the number of simulation dates, N_{node}, the total number of nodes, T, the simulation time length, and t_{step}, the simulation time step (60 s). In addition, $\triangle V_{\mathrm{d,n}}$ is the voltage deviation of each day, d, and node, n. When multiple control parameter sets minimize the summation of the voltage deviations, the last control parameter set is employed. The voltage deviation at each occurrence is described by (9). The optimal value of V_{devi} is zero, which represents the case of no voltage deviation.

B. Control Parameters Selection for SVR and SVC

The SVR or SVC is installed after the OLTC control method is upgraded to the centralized control method. The SVR and SVC control parameters are determined for the states in which the voltage deviation occurs with OLTC control. The objective function for the SVC is given by (8), which is same as that of the LDC method. However, K_p and K_{i} are used as control parameters instead of V_{tar}, R_{ref}, and X_{ref}.

IV. Numerical Simulations

Numerical simulations were performed to evaluate the voltage control performance of each of the aforementioned methods based on the limit of the PV penetration rate.

A. Settings of the Numerical Simulation

The model of the distribution system consists of two residential feeders. The summed load of certain feeders was set for realistic OLTC operations as shown in Fig. 3. The configuration of feeders A and B were identical [35]; however, the PV systems were interconnected only with feeder A. The summed load profile was calculated by subtracting the loads of feeders A and B from the actual measured substation profile. The trunk line length of feeders A and B was 3.65 km with loads of 2,000 households, which were connected to nodes. The lag power factor of both feeders was 0.98, while the power factor of the PV system was 1.

TABLE I
Verification Cases and Control Method

Case Number	Voltage Control Equipment		
	OLTC (Three methods)	SVC	SVR
Case 1 (only OLTC)	1	No installation	No installation
Case 2 (with SVC at end point)	1	1	No installation
Case 3 (with SVR at starting point)	1	No installation	1

TABLE II
Settings of the Numerical Simulation

Content		Setting Value
Simulation time step [s]		60
Rating voltage [V]		6600
Admissible voltage range [p.u.] (V_{low}–V_{up}) [36]		0.981–1.019
Number of simulation dates (N_{date}) (Two representative seasons have 4 days) (PV generation (3 days) and no PV generation (1 day))		8
Total number of nodes (N_{node}) (Feeders A and B have 28 nodes, respectively)		56
Peak values	Summed load [kW]	12789
	Load of household [kVA]	1
	PV system for household [kW]	2.77
OLTC	Rated capacity [MVA]	20
	Percent of reactance at the rated capacity [%]	15
	Voltage change per tap [p.u.] (V_{TC}) [37]	0.0091
	Dead band of the LDC method [p.u.] (Target voltage ± dead band width)	V_{tar} $\pm 0.01 V_{\mathrm{tar}}$
	Dead band of the centralized control method [p.u.] ($V_{\mathrm{low}}^{\mathrm{TC}}$–$V_{\mathrm{up}}^{\mathrm{TC}}$)	0.982–1.018
SVR	Rated capacity [MVA]	10
	Percent of reactance at the rated capacity [%]	1.5
	Voltage change per tap [p.u.] (V_{TC})	0.0151
	Dead band of the centralized control method [p.u.] ($V_{\mathrm{low}}^{\mathrm{TC}}$–$V_{\mathrm{up}}^{\mathrm{TC}}$)	0.982–1.018
SVC	Maximum output [kvar]	600
	Dead band [p.u.] ($V_{\mathrm{low}}^{\mathrm{SVC}}$–$V_{\mathrm{up}}^{\mathrm{SVC}}$)	0.990–1.010

Table I lists the number of voltage control instruments in each verification case while Table II lists the numerical simulation settings. In case 1, only the OLTC was used for voltage control. In cases 2 and 3, the SVC or SVR was installed in addition to the OLTC. Each piece of equipment was installed at the location that maximized the limit of the PV penetration rate. The SVC was installed at the end of the distribution trunk line (case 2), while the SVR was installed at the starting point. The dead band width of the LDC method was determined by consulting with specific power companies in Japan.

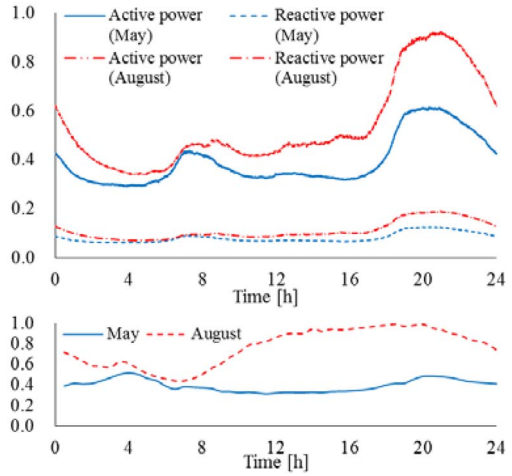

Fig. 4. Load profiles: low voltage load per household (top); summed load (bottom).

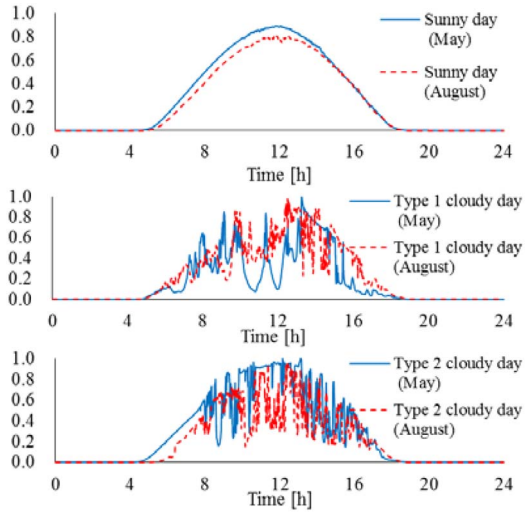

Fig. 5. PV output profiles per household: sunny day (top), type 1 cloudy day (middle), type 2 cloudy day (bottom).

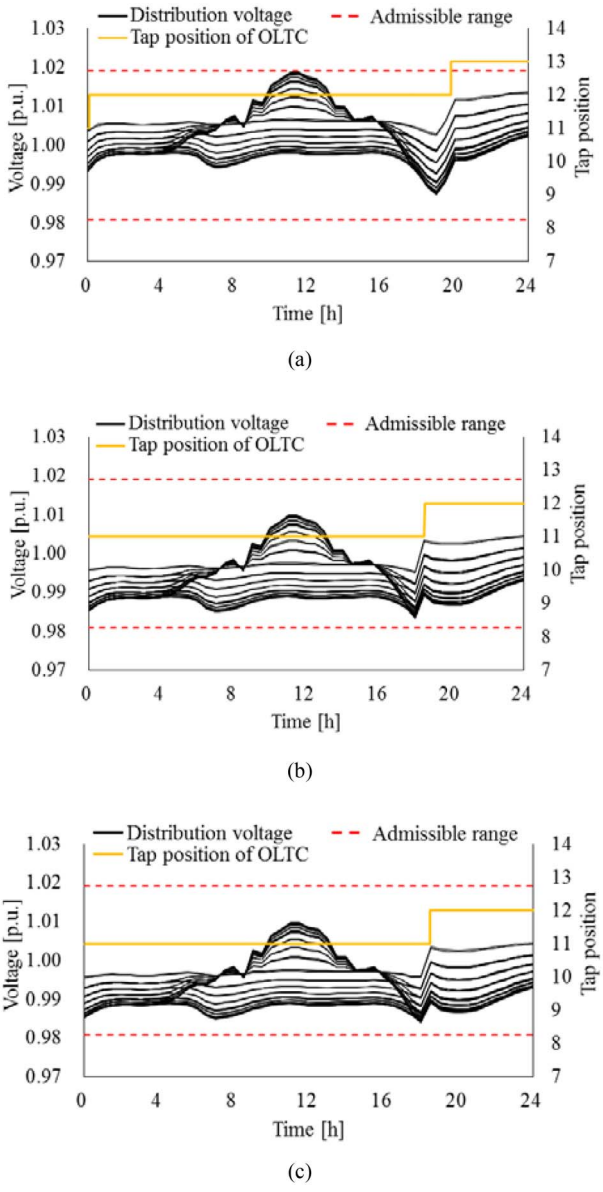

Fig. 6. Average voltage profiles (case 1, type 2 cloudy day, May, PV 40%): (a) scalar LDC method, (b) vector LDC method, (c) centralized control method.

For the centralized control method, the dead band was adjusted to minimize the tap change and avoid voltage deviation.

In this study, six types of PV profiles and two types of load profiles were assumed. Fig. 4 shows the profiles of the low voltage loads (top) and the summed load (bottom) with lagging reactive power. Fig. 5 shows the output profiles of a PV system for a household on a sunny day and two types of cloudy days during two representative seasons. Same load and PV profiles were used for each household to simulate the most severe conditions. All PV and load profiles were actually measured on site, and the PV profiles of households were referenced from the work: "Demonstrative Research on Grid-interconnection of Clustered Photovoltaic Power Generation Systems," which was organized by the New Energy and Industrial Technology Development Organization (NEDO) [38]. The features of each PV profile were as follows. On a sunny day, the PV output was stable. On a type 1 cloudy day, the amount of output fluctuation was drastic, while on a type 2 cloudy day, the number of PV fluctuations was high.

To realize an ideal centralized control, switches with sensors were installed at nodes where the distribution voltage was maximum or minimum at each PV penetration level. Previously, the installation locations of switches with sensors were determined by calculating the power flow under a 100% PV penetration rate. The voltage control performance of each method was evaluated based on the limit of the PV penetration rate. The PV penetration rate is defined as the ratio of the number of households with PV systems to the total number of households. The rate was specified as increasing in increments of 5% starting from zero. The 30-min averaged of each node voltage was used to determine the voltage deviation [39].

B. Analysis of Distribution Voltage Control

Fig. 6 shows the voltage profiles of all the nodes of the scalar LDC, vector LDC, and centralized control methods for

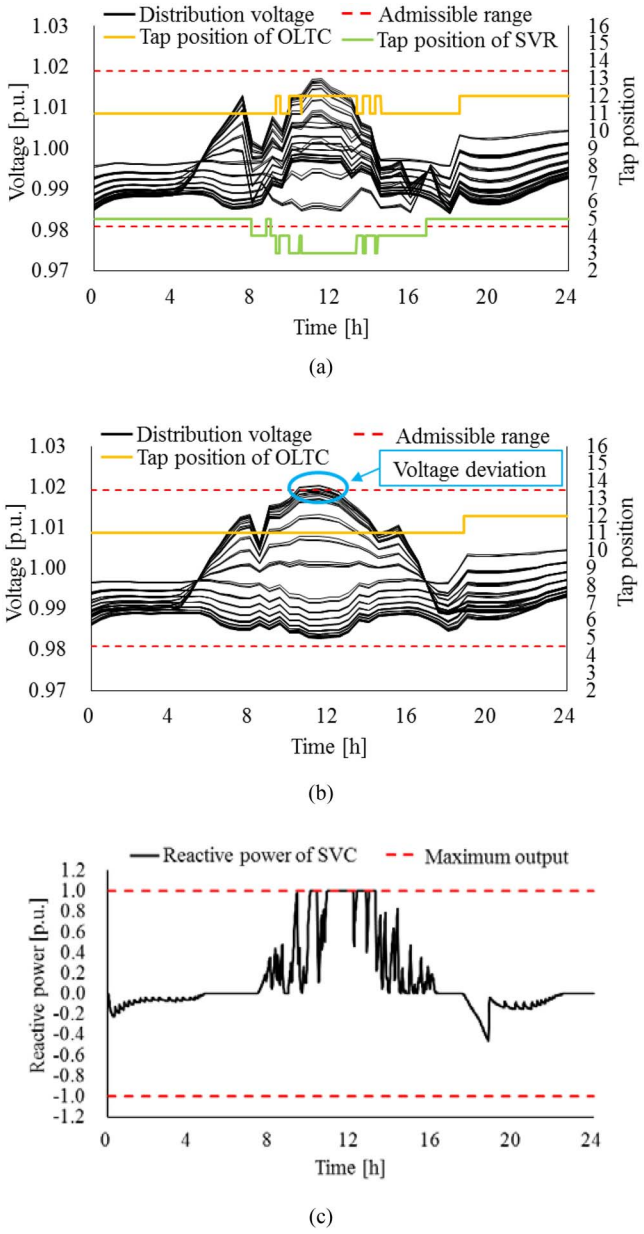

Fig. 7. Average voltage profiles and reactive power profile (centralized control method, type 2 cloudy day, May, PV 100%): (a) case 3, (b) case 2, (c) reactive power of SVC of (b).

case 1. In Fig. 6(a), the maximum distribution voltage is close to the upper limit of the admissible range. The OLTC tap position in the scalar LDC method during the day is 12. In Fig. 6(b), the distribution voltage is closer to the lower limit of the admissible range. The OLTC tap position of the vector LDC method is lower than that of the scalar LDC method because the control parameters of the vector LDC method were determined assuming PV penetration rate, unlike the scalar LDC method. The control parameters are compared as follows. The simulated line resistance and reactance were almost the same in both LDC methods. The target voltage of the reference point was 6636.7 V in the scalar LDC method and 6618.5 V in the vector LDC method. For Figs. 6(b) and (c), the tap transitions of the vector LDC and centralized control methods

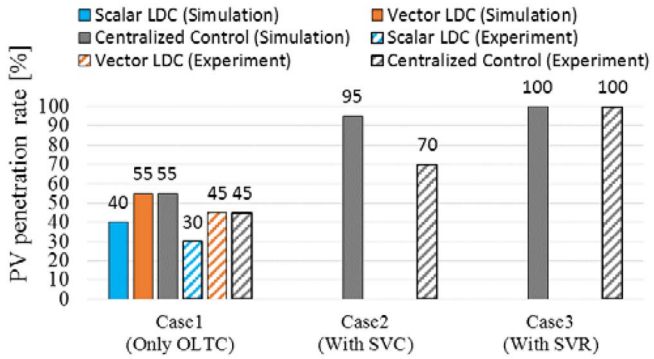

Fig. 8. Limit of the PV penetration rate with the numerical simulation and experiment (30-min averaged voltage was used to determine the voltage deviation).

are similar; therefore, the PV penetration rates of both methods are the same in case 1.

The voltage control performances of the SVC and SVR, the voltage profiles, and the reactive power profiles for cases 2 and 3 were compared as shown in Fig. 7. The distribution voltage was managed by OLTC and SVR controls, as shown in Fig. 7(a). Figs. 7(b) and (c) indicate that the distribution voltage deviates from the admissible range in spite of the maximum reactive power output by the SVC.

C. PV Penetration Rate

By analyzing the distribution voltage control in each case, the PV penetration rate was obtained. Fig. 8 shows the common limit of the PV penetration rate, which was the minimum installation rate achieved by any method in the six days of studies. The figure shows two additional findings.

First, except for Case 1 of the vector LDC and the centralized control methods, the limit of the PV penetration rate increased as the voltage control method of the OLTC was upgraded. This was analyzed as follows. The PV penetration rate obtained using the vector LDC method was higher than that obtained using the scalar LDC method by 15% because the control parameters of the vector LDC method were determined using the load current with PV systems.

Second, the limit of the PV penetration rate increased from case 1 to case 3. Installing the SVR at the starting point of the distribution system increased the limit of the PV penetration rate by 5% compared to installing the SVC at the end of the distribution system because the SVR controlled the whole distribution voltage, unlike the SVC.

The following conclusions can be drawn based on the results shown in Fig. 8 for the upgrade of the voltage control method. The OLTC control method with the scalar LDC method could manage a PV penetration rate of up to 40%; after which, the OLTC control method should be upgraded to the vector LDC method, which requires no sensor installation, unlike the centralized control method. When the PV penetration rate exceeded 55%, none of the OLTC control methods could avoid voltage deviation, and SVC or SVR installation was necessary.

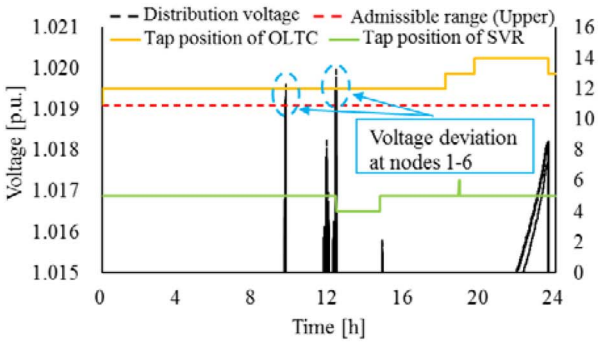

(a)

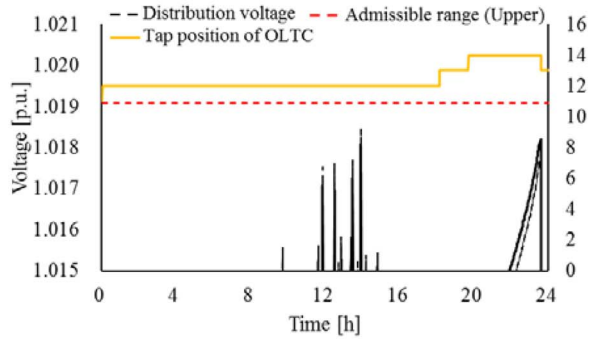

(b)

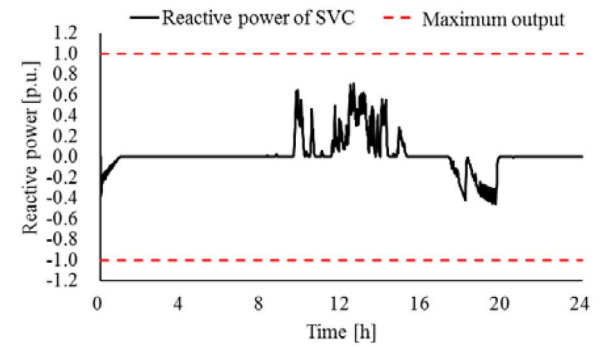

(c)

Fig. 9. Instantaneous voltage and reactive power profiles (type 1 cloudy day, August, PV 65%): (a) voltage in case 3, (b) voltage in case 2, and (c) reactive power of SVC of (b).

As shown in Fig. 6, using the SVR increased the PV penetration rate more than using the SVC. Thus, SVR installation was selected as the more suitable method.

D. Comparison of SVR and SVC

The voltage control performances were compared in terms of the 30-min averaged voltage and the 60-s values used to check the instantaneous voltage deviation (i.e., the step size of the used profiles). Fig. 9 shows the instantaneous voltage profiles for the type 1 cloudy day in August. As shown in Fig. 9(a), the voltages at nodes one to six in Fig. 3 deviate above the upper limit twice. However, no distribution voltage deviates below the lower limit. Figs. 9(b) and (c) show that

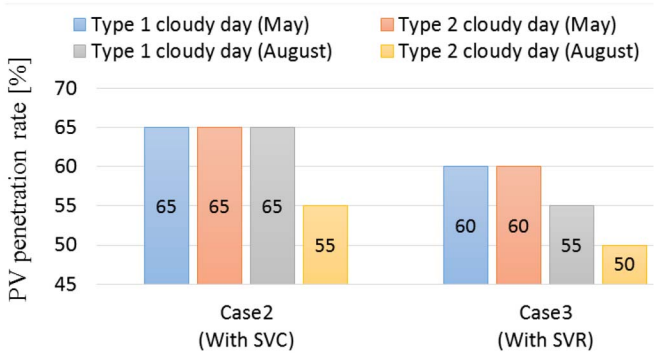

Fig. 10. Limit of the PV penetration rate with the numerical simulation (instantaneous voltage was used to determine the voltage deviation).

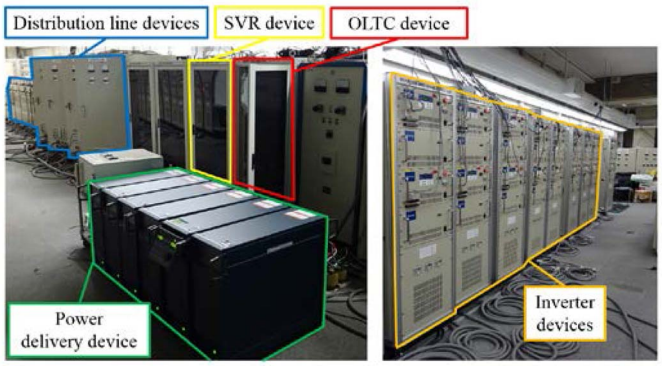

Fig. 11. ANSWER devices.

the instantaneous voltage is maintained within the admissible range with SVC control. Fig. 10 shows the PV penetration rate with centralized control in cases 2 and 3 for two types of cloudy days. The SVC increases the PV penetration rate more than the SVR, because the former controls rapid voltage fluctuations, unlike the latter. This phenomenon is confirmed by Fig. 9. Based on the results of the numerical simulations, the SVR was more effective than the SVC in extending the PV penetration rate while preventing 30-min averaged voltage deviations. The SVC on the other hand, helped increase the PV penetration rate while preventing instantaneous voltage deviations.

V. Experiment With a Test Bed Active Network Simulator With Energy Resources (ANSWER)

An experiment with an Active Network Simulator with Energy Resources (ANSWER) [40] was performed to confirm the validity of the proposed scheme in parallel with the numerical simulations.

A. Experiment Settings

ANSWER was used to shape the experimental distribution system, which was a model of an actual 6.6-kV distribution system scaled down to 200-V. Fig. 11 depicts ANSWER. The currents passing through each piece of equipment and the bus voltage were 1/25 and 1/33 of the actual 6.6-kV distribution system, respectively. The experimental distribution system was

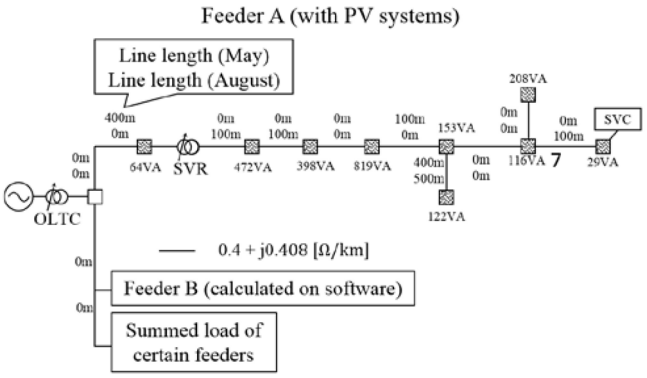

Fig. 12. Distribution system model of ANSWER.

TABLE III
SETTINGS OF THE EXPERIMENT

CONTENT		Setting Value
Simulation time step [s]		60
Rating voltage [V]		200
Admissible voltage range [p.u.] (V_{low}–V_{up})		0.981–1.019
Number of simulation dates (N_{date}) (Two representative seasons have 4 days) (PV generation (3 days) and no PV generation (1 day))		8
Total number of nodes (N_{node}) (Feeders A and B have 9 nodes, respectively)		18
Peak values	Summed load [kW]	15.5
	Load of household [VA]	1.21
	PV system for household [W]	3.35
OLTC	Rated capacity [kVA]	20
	Voltage change per tap [p.u.] (V_{TC})	0.0091
	Dead band of the LDC method [p.u.] (Target voltage ± dead band width)	V_{tar} $\pm 0.01 V_{tar}$
	Dead band of the centralized control method [p.u.] (V_{low}^{TC}–V_{up}^{TC})	0.982–1.018
SVR	Rated capacity [kVA]	20
	Voltage change per tap [p.u.] (V_{TC})	0.0151
	Dead band of the centralized control method [p.u.] (V_{low}^{TC}–V_{up}^{TC})	0.982–1.018
SVC	Maximum output [kvar]	600
	Dead band [p.u.] (V_{low}^{SVC}–V_{up}^{SVC})	0.990–1.010

comprised of the power delivery device, the OLTC and SVR devices, ten distribution line devices, ten inverter devices that simulated the load, PV systems, and the SVC. The voltage values of each distribution line device and the feeder B were used for the centralized control method. Fig. 12 shows the distribution system model of ANSWER. The distribution voltage of feeder B was calculated by the numerical simulation.

The experimental settings are as listed in Table III. The control parameters of the OLTC, SVR, and SVC were determined as follows. A model of the distribution system was developed on a computer to optimize the control parameters of the ANSWER system. The line lengths were adjusted to match the most severe points of the distribution voltage, such as the maximum or minimum voltage in the experimental and modeled systems. The control parameters were then calculated as described in Section III. When the distribution voltage deviated from the admissible range using the control parameters optimized on the computer, the control parameters were adjusted.

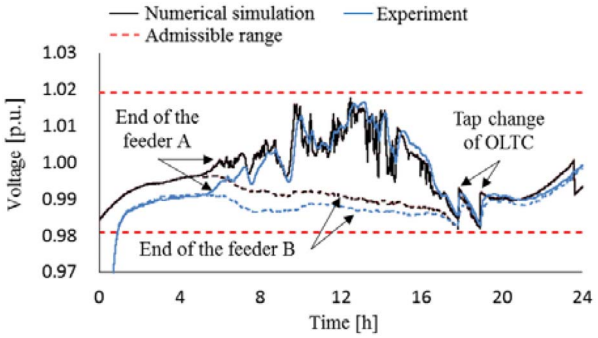

Fig. 13. Comparison of the distribution voltage of the numerical simulation with that of the experiment (case 1, type 1 cloudy day, August, PV 50%).

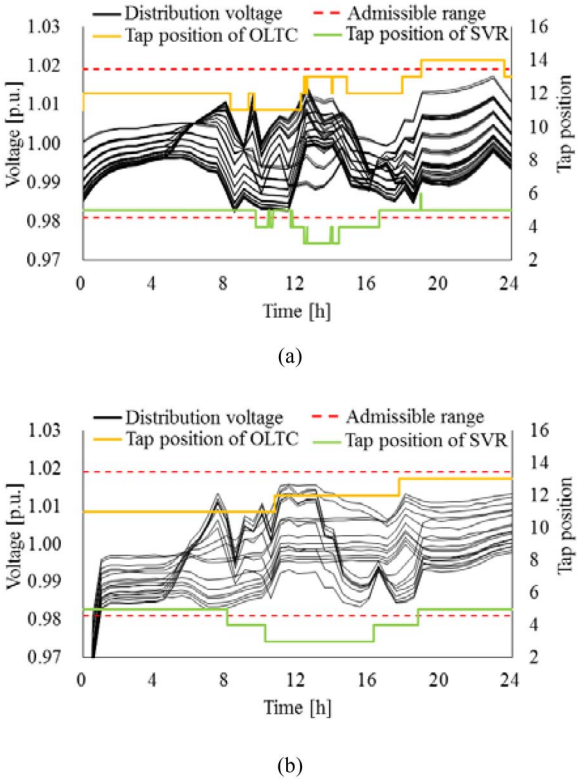

Fig. 14. Comparison of (a) numerical simulation and (b) experimental results of distribution voltage and tap operation (centralized control method, case 3, type 1 cloudy day, May, PV 100%).

B. Comparison of the Numerical Simulation and Experimental Results

To analyze the difference between the PV penetration levels of the numerical simulation and those of the experiment, the distribution voltages were compared. Fig. 13 shows the distribution voltage at the end of feeders A and B obtained in the numerical simulation and experiment for case 2 with the centralized control method and a PV penetration rate of 50%. ANSWER is a 200-V distribution system. Thus, the distribution voltage of ANSWER was 33 times that of the numerical simulation. The trend of voltage profiles for the numerical simulation and ANSWER were consistent. The voltage difference reached 0.015 p.u. at the maximum. The difference in distribution voltage between the numerical simulation and the

experiment may have decreased the limit of the PV penetration rate of the experiment. However, the limit of the PV penetration rate of the numerical simulation and experiment was the same as in case 3, as shown in Fig. 8. The SVR controlled the whole distribution voltage in feeder A, and therefore, the difference in distribution voltage in feeders A and B was reduced. Thus, the limit of the PV penetration rate reached 100% in the numerical simulation and experiment.

Fig. 14 shows the numerical simulation and experimental results for case 3. Both distribution voltage profiles were maintained within the admissible range. The operation of the OLTC and SVR in Figs. 14(a) and (b) were different since the voltage range of the numerical simulation was narrower than that of the experiment; therefore, the OLTC and SVR could frequently change the tap position in the numerical simulation.

The experimental results show the same trend as the numerical simulation in cases 1 and 2, as shown in Fig. 8. The limit of the PV penetration rate of experiment decreased from 10% to 25% compared to that of the numerical simulation. This decrease could be traceable to the differences in voltage distribution occasioned by the differences in the line impedances used in the numerical simulation and the experiment.

VI. Conclusion

In this study, we devised a comprehensive scheme to determine a suitable method and timing for upgrading the voltage control method. The proposed scheme shows a suitable voltage control method and timing for upgrading the OLTC control method, and the additional installation of the SVC or SVR based on the limit of the PV penetration rate. This limit with voltage control methods was calculated through numerical simulations and experiments with an active network simulator with energy resources (ANSWER). The tendencies of the PV penetration rate increase and distribution voltage profiles were consistent, validating the numerical simulation results. The results showed that the SVR increases the PV penetration rate more than the SVC, while preventing deviations of the 30-min averaged voltage. On the other hand, the SVC helped increase PV penetration while preventing instantaneous voltage deviations. Thus, this work demonstrates the necessity of controlling the SVR and SVC to increase PV penetration while avoiding instantaneous voltage deviations. The proposed method was used in a distribution system consisting of two feeders. A future study will be conducted to confirm the effectiveness of this method in a large-scale distribution system. Meanwhile, the proposed scheme is applicable to any distribution system and any voltage control method. This study could thus contribute toward expanding the hosting capacities of distribution PV systems.

Acknowledgment

This research was part of the "Next-generation optimizing control technique demonstration project for power transmission and distribution systems." S. Akagi acknowledges the Leading Graduate Program in Science and Engineering, Waseda University from MEXT, Japan.

References

[1] S. Esterly, *Renewable Energy Data Book*, Nat. Renew. Energy Lab., Golden, CO, USA, Nov. 2015. [Online]. Available: http://www.nrel.gov/docs/fy16osti/64720.pdf

[2] *Tracking Clean Energy Progress 2015*, Int. Energy Agency, Paris, France, May 2015 [Online]. Available: https://www.iea.org/etp/tracking2015/

[3] Feed-in Tariff Information: Website for Information Publication. *Ministry of Economy, Trade and Industry (METI)*. Accessed on Dec. 10, 2016. [Online]. Available: http://www.fit.go.jp/statistics/public_sp.html

[4] *Long-Range Estimate of Energy Supply and Demand-Related*, Ministry Econ. Trade Ind., Tokyo, Japan, Jul. 2016. [Online]. Available: http://www.enecho.meti.go.jp/committee/council/basic_policy_subcommittee/mitoshi/011/pdf/011_07.pdf

[5] M. Rylander, L. Rogers, and J. Smith, "Distribution feeder hosting capacity: What matters when planning for DER?" Elect. Power Res. Inst., Inc., Knoxville, TN, USA, Apr. 2015.

[6] M. Rylander, "Determining the effectiveness of feeder clustering techniques for identifying hosting capacity for DER," Elect. Power Res. Inst., Inc., Knoxville, TN, USA, Nov. 2015.

[7] S. Wang, S. Chen, L. Ge, and L. Wu, "Distributed generation hosting capacity evaluation for distribution systems considering the robust optimal operation of OLTC and SVC," *IEEE Trans. Sustain. Energy*, vol. 7, no. 3, pp. 1111–1123, Jul. 2016.

[8] N. Jayasekara, M. A. S. Masoum, and P. J. Wolfs, "Optimal operation of distributed energy storage systems to improve distribution network load and generation hosting capability," *IEEE Trans. Sustain. Energy*, vol. 7, no. 1, pp. 250–261, Jan. 2016.

[9] F. Capitanescu, L. F. Ochoa, H. Margossian, and N. D. Hatziargyriou, "Assessing the potential of network reconfiguration to improve distributed generation hosting capacity in active distribution systems," *IEEE Trans. Power Syst.*, vol. 30, no. 1, pp. 346–356, Jan. 2015.

[10] S.-J. Huang, C.-W. Hsieh, and H.-H. Wan, "Confirming the permissible capacity of distributed generation for grid-connected distribution feeders," *IEEE Trans. Power Syst.*, vol. 30, no. 1, pp. 540–541, Jan. 2015.

[11] A. Navarro-Espinosa and L. F. Ochoa, "Increasing the PV hosting capacity of LV networks: OLTC-fitted transformers vs. reinforcements," in *Proc. IEEE PES ISGT*, Washington, DC, USA, Feb. 2015, pp. 1–5.

[12] X. Liu, A. Aichhorn, L. Liu, and H. Li, "Coordinated control of distributed energy storage system with tap changer transformers for voltage rise mitigation under high photovoltaic penetration," *IEEE Trans. Smart Grid*, vol. 3, no. 2, pp. 897–906, Jun. 2012.

[13] N. Yorino, Y. Zoka, M. Watanabe, and T. Kurushima, "An optimal autonomous decentralized control method for voltage control devices by using a multi-agent system," *IEEE Trans. Power Syst.*, vol. 30, no. 5, pp. 2225–2233, Sep. 2015.

[14] M. Kim, R. Hara, and H. Kita, "Design of the optimal ULTC parameters in distribution system with distributed generations," *IEEE Trans. Power Syst.*, vol. 24, no. 1, pp. 297–305, Feb. 2009.

[15] M. E. Elkhatib, R. El-Shatshat, and M. M. A. Salama, "Novel coordinated voltage control for smart distribution networks with DG," *IEEE Trans. Smart Grid*, vol. 2, no. 4, pp. 598–605, Dec. 2011.

[16] C. Gao and M. A. Redfern, "A review of voltage control techniques of networks with distributed generations using on-load tap changer transformers," in *Proc. Univ. Power Eng. Conf.*, Cardiff, U.K., 2010, pp. 1–6.

[17] D. Ranamuka, A. P. Agalgaonkar, and K. M. Muttaqi, "Online voltage control in distribution systems with multiple voltage regulating devices," *IEEE Trans. Sustain. Energy*, vol. 5, no. 2, pp. 617–628, Apr. 2014.

[18] C. Gao and M. A. Redfern, "Advanced voltage control strategy for on-load tap-changer transformers with distributed generations," in *Proc. Univ. Power Eng. Conf.*, Soest, Germany, 2011, pp. 1–6.

[19] T. Stetz *et al.*, "Techno-economic assessment of voltage control strategies in low voltage grids," *IEEE Trans. Smart Grid*, vol. 5, no. 4, pp. 2125–2132, Jul. 2014.

[20] A. T. Procopiou, C. Long, and L. F. Ochoa, "On the effects of monitoring and control settings on voltage control in PV-rich LV networks," in *Proc. IEEE Power Energy. Soc. Gen. Meeting*, Denver, CO, USA, 2015, pp. 1–5.

[21] C. Long, A. T. Procopiou, L. F. Ochoa, G. Bryson, and D. Randles, "Performance of OLTC-based control strategies for LV networks with photovoltaics," in *Proc. IEEE Power Energy. Soc. Gen. Meeting*, Denver, CO, USA, 2015, pp. 1–5.

[22] C. Long and L. F. Ochoa, "Voltage control of PV-rich LV networks: OLTC-fitted transformer and capacitor banks," *IEEE Trans. Power Syst.*, vol. 31, no. 5, pp. 4016–4025, Sep. 2016.

[23] K. M. Muttaqi, A. D. T. Le, M. Negnevitsky, and G. Ledwich, "A coordinated voltage control approach for coordination of OLTC, voltage regulator, and DG to regulate voltage in a distribution feeder," *IEEE Trans. Ind. Appl.*, vol. 51, no. 2, pp. 1239–1248, Mar./Apr. 2015.

[24] J.-H. Choi and S.-I. Moon, "The dead band control of LTC transformer at distribution substation," *IEEE Trans. Power Syst.*, vol. 24, no. 1, pp. 319–326, Feb. 2009.
[25] C.-S. Chen, C.-H. Lin, W.-L. Hsieh, C.-T. Hsu, and T.-T. Ku, "Enhancement of PV penetration with DSTATCOM in Taipower distribution system," *IEEE Trans. Power Syst.*, vol. 28, no. 2, pp. 1560–1567, May 2013.
[26] M. J. E. Alam, K. M. Muttaqi, and D. Sutanto, "A multi-mode control strategy for VAr support by solar PV inverters in distribution networks," *IEEE Trans. Power Syst.*, vol. 30, no. 3, pp. 1316–1326, May 2015.
[27] P. Jahangiri and D. C. Aliprantis, "Distributed volt/VAr control by PV inverters," *IEEE Trans. Power Syst.*, vol. 28, no. 3, pp. 3429–3439, Aug. 2013.
[28] Z. Ziadi *et al.*, "Optimal voltage control using inverters interfaced with PV systems considering forecast error in a distribution system," *IEEE Trans. Sustain. Energy*, vol. 5, no. 2, pp. 682–690, Apr. 2014.
[29] M. Parniani and M. R. Iravani, "Voltage control stability and dynamic interaction phenomena of static VAR compensators," *IEEE Trans. Power Syst.*, vol. 10, no. 3, pp. 1592–1597, Aug. 1995.
[30] T. Senjyu, Y. Miyazato, A. Yona, N. Urasaki, and T. Funabashi, "Optimal distribution voltage control and coordination with distributed generation," *IEEE Trans. Power Del.*, vol. 23, no. 2, pp. 1236–1242, Apr. 2008.
[31] F. A. Viawan and D. Karlsson, "Voltage and reactive power control in systems with synchronous machine-based distributed generation," *IEEE Trans. Power Del.*, vol. 23, no. 2, pp. 1079–1087, Apr. 2008.
[32] Y. P. Agalgaonkar, B. C. Pal, and R. A. Jabr, "Distribution voltage control considering the impact of PV generation on tap changers and autonomous regulators," *IEEE Trans. Power Syst.*, vol. 29, no. 1, pp. 182–192, Jan. 2014.
[33] P. S. Sensarma, K. R. Padiyar, and V. Ramanarayanan, "Analysis and performance evaluation of a distribution STATCOM for compensating voltage fluctuations," *IEEE Trans. Power Del.*, vol. 16, no. 2, pp. 259–264, Apr. 2001.
[34] N. Daratha, B. Das, and J. Sharma, "Coordination between OLTC and SVC for voltage regulation in unbalanced distribution system distributed generation," *IEEE Trans. Power Syst.*, vol. 29, no. 1, pp. 289–299, Jan. 2014.
[35] Electric Technology Research Association, "Harmonic failure prevention measures of the distribution system," *Denkikyoudoukenkyu*, vol. 37, no. 3, p. 102, Oct. 1981.
[36] Y. Isozaki *et al.*, "Detection of cyber attacks against voltage control in distribution power grids with PVs," *IEEE Trans. Smart Grid*, vol. 7, no. 4, pp. 1824–1835, Jul. 2016.
[37] *Electrical Engineering Handbook*, 7th ed., Ohmsha, Ltd., Chiyoda-ku, Tokyo, 2013, p. 1281.
[38] *Demonstrative Research on Clustered PV Systems*. Accessed on Dec. 10, 2016. [Online]. Available: http://www.nedo.go.jp/activities/ZZ_00229.html
[39] *Electricity Business Act Enforcement Regulations Information*, Ministry Econ. Trade Ind., Tokyo, Japan, accessed on Dec. 10, 2016. [Online]. Available: http://law.e-gov.go.jp/htmldata/H07/H07F03801000077.html
[40] S. Yoshizawa *et al.*, "Voltage control of multiple step voltage regulators by renewing control parameters," in *Proc. Power Syst. Comput. Conf. (PSCC)*, Wrocław, Poland, 2014, pp. 1–7.

Satoru Akagi (S'15) received the B.Eng. degree in electrical engineering and bioscience from Waseda University, Japan, in 2014, where he is currently pursuing the Ph.D. degree in electrical power engineering. His research interests include cooperative control of distributed generation and distribution systems.

Ryo Takahashi received the B.Eng. and M.Eng. degrees from Waseda University, Japan, in 2014 and 2016, respectively. His research interest includes voltage control in distribution systems with distributed generators.

Akihisa Kaneko was born in Ibaraki, Japan, in 1993. He received the B.Eng. degree in electrical engineering and bioscience from Waseda University, Tokyo, Japan, in 2016, where he is currently pursuing the graduation degree. His research field is voltage control in distribution systems with distributed generators.

Masakazu Ito received the Ph.D. degree from the Tokyo University of Agriculture and Technology. He is an Associate Professor with the Advanced Collaborative Research Organization for Smart Society, Waseda University, Japan. He is studying smart grid technologies, especially those with PV systems and energy storages. He started as an Assistant Professor with the Tokyo Institute of Technology, and then became a JSPS Research Fellow with the CEA, INES, France, researching the life cycle analysis and remote sensing for very large scale photovoltaic systems.

Jun Yoshinaga received the M.Eng. degree from Osaka University, Japan, in 1994, and the Ph.D. degree from Waseda University, Japan, in 2016. In 1994, he became an Engineer with Tokyo Electric Power Company. In 2012, he also became a Researcher with Research Institute for Advanced Network Technology, Waseda University. His research fields of interest are optimization of distribution systems and control concerned with renewable energy sources and demand response.

Yasuhiro Hayashi (M'91) received the B.Eng., M.Eng., and D.Eng. degrees from Waseda University, Japan, in 1989, 1991, and 1994, respectively. In 1994, he became a Research Associate with Ibaraki University, Mito, Japan. In 2000, he became an Associate Professor with the Department of Electrical and Electronics Engineering, Fukui University, Fukui, Japan. He has been with the Department of Electrical Engineering and Bioscience, Waseda University as a Professor since 2009, where he has been the Director of the Research Institute of Advanced Network Technology since 2010. Since 2014, he has been the Dean of the Advanced Collaborative Research Organization for Smart Society, Waseda University. His current research interests include optimization of distribution system operation and forecasting, operation, planning, and control concerned with renewable energy sources and demand response. He is a member of the Institute of Electrical Engineers of Japan and the International Council on Large Electric Systems.

Hiroshi Asano (M'88) received the B.Eng., M.Eng., and D.Eng. degrees in electrical engineering from the University of Tokyo. He is currently a Guest Professor with Waseda University, the Deputy Associate Vice President with Central Research Institute of Electric Power Industry, a Visiting Professor with the University of Tokyo, and a professor with the Tokyo Institute of Technology. His research interests include systems analysis of demand response, smart grid, distributed energy resources, and power markets. He has been a member of CIGRE, IEEJ, JSER, and IAEE.

Hiromi Konda is a Manager with the Business Planning Office, TEPCO Power Grid, Inc., Japan. He is studying smart grid technologies, especially those control methods of electric power systems with a large amount of renewable energies.